

1 **Title:**

2

3 Secular change and inter-annual variability of the Gulf Stream position, 1993-2013, 70°-55° W

4

5 **Authors:**

6

7 James J. Bisagni<sup>1</sup> and Avijit Gangopadhyay

8 University of Massachusetts, Dartmouth

9 School for Marine Science and Technology

10 200 Mill Rd., Suite 325

11 Fairhaven, MA, USA

12 02719

13

14 Alejandra Sanchez-Franks

15 National Oceanography Centre

16 Southampton, UK

17 SO14 3ZH

18

19 <sup>1</sup>Corresponding Author: [jbisagni@umassd.edu](mailto:jbisagni@umassd.edu), (508) 910-6328

20

20 **Abstract:**

21

22 The Gulf Stream (GS) is the northeastward-flowing surface limb of the Atlantic Ocean's  
23 meridional overturning circulation (AMOC) "conveyor belt" that flows towards Europe and the  
24 Nordic Seas. Changes in the GS position after its separation from the coast at Cape Hatteras, i.e.,  
25 from 75°W to 50°W, may be key to understanding the AMOC, sea level variability and  
26 ecosystem behavior along the east coast of North America. In this study we compare secular  
27 change and inter-annual variability (IAV) of the Gulf Stream North Wall (GSNW) position with  
28 equator-ward Labrador Current (LC) transport along the southwestern Grand Banks near 52° W  
29 using 21 years (1993-2013) of satellite altimeter data. Results at 55°, 60°, and 65° W show a  
30 significant southward (negative) secular trend for the GSNW, decreasing to a small but  
31 insignificant southward trend at 70° W. IAV of de-trended GSNW position residuals also  
32 decreases to the west. The long-term secular trend of annual mean upper layer (200 m) LC  
33 transport near 52° W is positive. Furthermore, IAV of LC transport residuals near 52° W along  
34 the southwestern Grand Banks are significantly correlated with GSNW position residuals at 55°  
35 W at a lag of +1-year, with positive (negative) LC transport residuals corresponding to  
36 southward (northward) GSNW positions one year later. The Taylor-Stephens index (TSI)  
37 computed from the first principal component of the GSNW position from 79° to 65° W shows a  
38 similar relationship with a more distal LC index computed along altimeter ground track 250  
39 located north of the Grand Banks across Hamilton Bank in the western Labrador Sea. Increased  
40 (decreased) sea height differences along ground track 250 are significantly correlated with a  
41 more southward (northward) TSI two years later (lag of +2-years). Spectral analysis of IAV  
42 reveals corresponding spectral peaks at 5-7 years and 2-3 years for the North Atlantic Oscillation  
43 (NAO), GSNW (70°-55°W) and LC transport near 52° W for the 1993-2013 period suggesting a  
44 connection between these phenomena. An upper-layer (200 m) slope water volume calculation  
45 using the LC IAV rms residual of +1.04 Sv near 52° W results in an estimated GSNW IAV  
46 residual of 79 km, or 63% of the observed 125.6 km (1.13°) rms value at 55° W. A similar  
47 upper-layer slope water volume calculation using the positive long-term, upper-layer LC  
48 transport trend accounts for 68% of the mean observed secular southward shift of the GSNW  
49 between 55° and 70°W over the 1993-2013 period. Our work provides additional observational  
50 evidence of important interactions between the upper layers of the sub-polar and sub-tropical  
51 gyres within the North Atlantic over both secular and inter-annual time scales as suggested by  
52 previous studies.

53

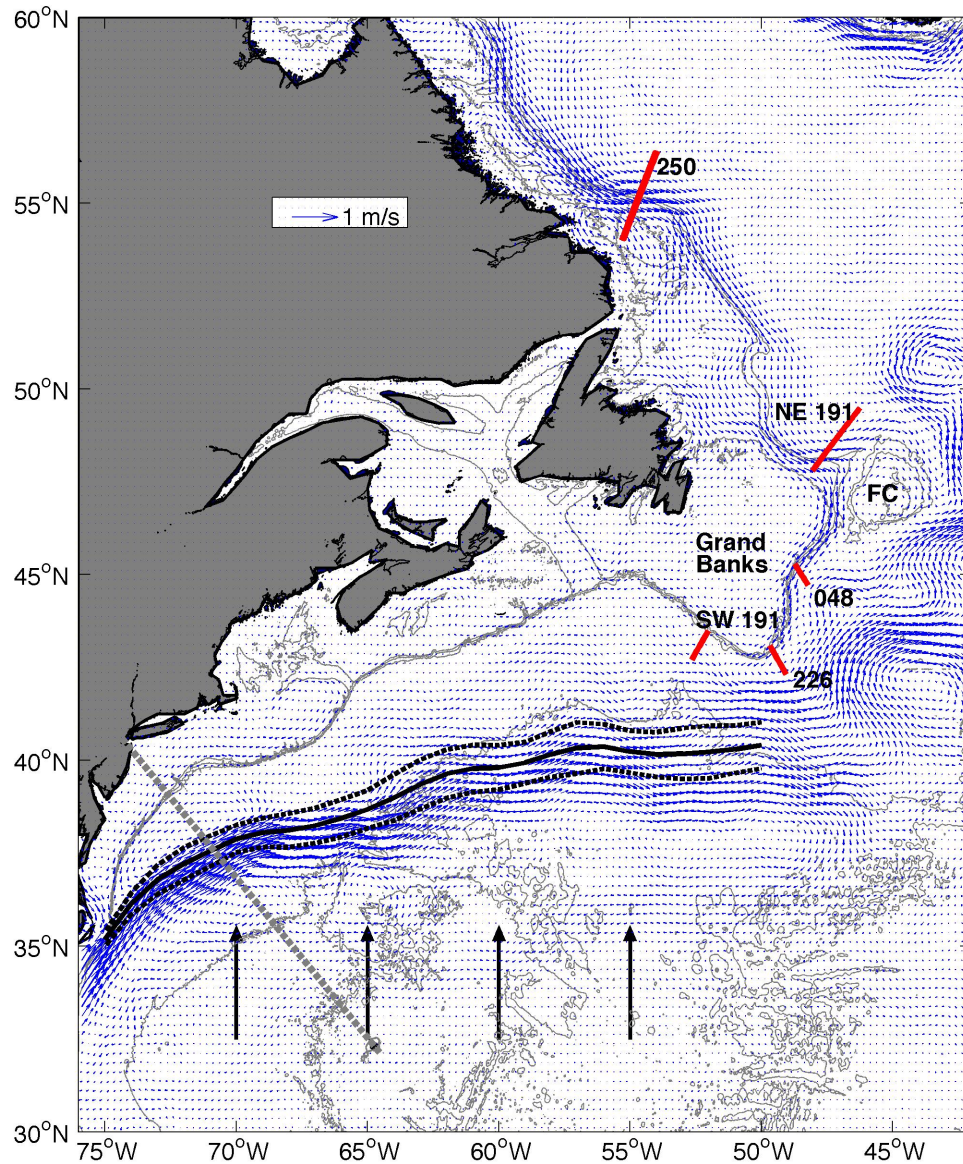
### 53 **Introduction:**

54

55 The Gulf Stream (GS) and Labrador Current (LC) form the western boundary currents of  
56 the sub-tropical and sub-polar gyres of the North Atlantic, respectively, meeting near the Tail of  
57 the Grand Banks (TGB). At the TGB, a large fraction of the LC turns eastward and joins the GS  
58 to form the North Atlantic Current (NAC) that continues flowing towards Europe and the Nordic  
59 Seas. The remaining LC fraction flows equator-ward around the TGB along the seaward edge of  
60 the Canadian and U.S. continental shelves. An examination of geostrophic surface velocity  
61 vectors (**Fig. 1**) (calculated from 1993-2013, Ssalto/Duacs altimetry products, *in situ* data,  
62 MSS\_CNES-CLS11 Mean Sea Surface, and the EGM-DIR-R4 geoid model, combining data  
63 from both GOCE and GRACE geoid models), clearly shows this general large-scale circulation  
64 in the western North Atlantic: the northeastward-flowing GS from Cape Hatteras to south of the  
65 TGB, its mean location observed in the large velocities located between the anti-cyclonic sub-  
66 tropical gyre and the Northern Recirculation Gyre (NRG). Moving north, at the TGB, the GS  
67 evolves into the meandering NAC, distending in and out of the Northwest Corner. Patterns of  
68 low dynamic height within the Labrador Basin are characteristic of the cyclonic sub-polar gyre  
69 with the LC flowing southeast and equatorward around the Grand Banks. The strongest LC  
70 signal is located along the 500 m isobath from the north just off Labrador near altimeter ground  
71 track 250, southward to the west of the Flemish Cap, and then around the Grand Banks (**Fig. 1**).  
72 Sinking of cold dense water in the Labrador Sea flows southward along the outer continental  
73 slope and rise (not shown) to form the Deep Western Boundary Current (DWBC), forming the  
74 southward-flowing subsurface limb of the Atlantic Ocean's meridional overturning circulation  
75 (AMOC), with the GS forming the AMOC's northward-flowing surface limb. Inputs from the  
76 Greenland, Iceland, and Norwegian Sea (not shown) also form an important southward-flowing  
77 sub-surface portion of the AMOC described in summary by Yashayaev *et al.* (2015).

78 The space-time variability of the latitudinal excursion of the GS "north wall" (GSNW) has  
79 been shown by combined observational and modeling studies to be an important diagnostic  
80 variable and indicator of the AMOC's amplitude (Joyce and Zhang, 2010; Sanchez-Franks and  
81 Zhang, 2015). A stronger (weaker) AMOC corresponded to a more southerly (northerly) GSNW  
82 using a GFDL climate model and satellite-derived data, respectively (Joyce and Zhang, 2010).  
83 Cooler temperatures, lower salinities, and low planetary potential vorticity characteristic of  
84 Labrador Sea Water (LSW), along with stronger southwestward flow, were in phase within  
85 Slope Waters located between the shelf break and the GSNW from 1993-2007, and preceded a  
86 southward shift of the GSNW by 6 months (Peña-Molino and Joyce, 2008) in agreement with  
87 Rossby (1999), Rossby and Benway (2000), and Flagg *et al.* (2006). Direct observations of the  
88 DWBC along the "Line-W" array located northwest of Bermuda show similar results with  
89 stronger DWBC transport when the GSNW is displaced to the south (Toole *et al.*, 2011). More  
90 recent studies have shown that in addition to seasonal and short timescale variability, strong  
91 inter-annual variability (IAV) of the AMOC has also occurred, with a 30% reduction in AMOC  
92 transport between 1 April 2009 and 31 March 2010 along the RAPID/WATCH 26°N  
93 measurement array (McCarthy *et al.*, 2012; Smeed *et al.*, 2014). This reduction in the AMOC  
94 was accompanied by a stronger Slope Water current, but does not support the Slope Current as a  
95 significant driver of GS position by itself, which may also partly result from the supply of source  
96 waters from the Labrador Sea and the sub-polar gyre (Rossby, 1999; Ezer and Atkinson, 2014;  
97 Ezer, 2015).

98



134 Figure 1. Mean geostrophic surface velocities showing the general large scale circulation and  
135 both the northeast-flowing Gulf Stream and southward-flowing Labrador Current (see text for  
136 explanation). Long-term mean position of the monthly-mean Gulf Stream North Wall (black  
137 solid line) and standard deviation (black dashed lines) are estimated from SST anomalies at  
138 every degree of longitude between 75° W and 50° W from the Canadian Marine Environmental  
139 Data Service. Also shown are the locations of: four longitude lines (black vertical arrows)  
140 which annual mean positions of the Gulf Stream North Wall were measured, five outer-shelf  
141 altimeter along-track segments (red lines) for measuring upper-layer Labrador Current transport  
142 or sea height, the *M/V Oleander* transect (gray dashed line), the location of the Grand Banks,  
143 the Flemish Cap (FC), and the 500 m, 1000 m and 5000 m isobaths.

144

144 Changes in the latitudinal excursion of the GS path and their impact on its cross-stream  
145 sea-level gradient have also been linked to sea level rise along the Canadian and U.S. east coasts,  
146 a possible “slowing” of the GS, and increased frequency of coastal flooding (Boon, 2012; Ezer  
147 and Corlett, 2012; Sallenger *et al.*, 2012; Ezer *et al.*, 2013; Ezer and Atkinson, 2014). The  
148 extreme sea level rise noted using tide gauge data for a northeast region located between Cape  
149 Hatteras and Newfoundland may result from remote wind forcing (Andres *et al.*, 2013) but also  
150 corresponded to the period of the 30% reduction in the AMOC from 2009-2010 (Goddard *et al.*,  
151 2015). Although both the GS and LC are driven by large-scale wind patterns over their  
152 respective gyres, with variability attributed to the North Atlantic Oscillation (NAO) (Taylor and  
153 Stephens, 1998; Marshall *et al.*, 2001) studies suggest that thermohaline interactions between the  
154 GS, LC, DWBC, recirculation gyres, and shelf waters may also be important (Rossby, 1999;  
155 Rossby and Benway, 2000; Marshall *et al.*, 2001, Chaudhuri *et al.*, 2011). A significant part of  
156 this thermohaline interaction may result directly from the remaining equator-ward-flowing  
157 fraction of the surface LC and shelf waters releasing varying amounts of less-saline waters into  
158 the Slope Sea.

159 Evidence from low-frequency variations of sea surface salinity (SSS) shows large IAV ( $\pm 1$ -  
160 2 PSU) that is coherent along the *M/V Oleander* line between New Jersey and Bermuda (Fig. 1)  
161 across both the continental shelf and slope water regions, supporting the hypothesis of a release  
162 of less-saline waters from the shelf into the Slope Sea (Rossby and Benway, 2000). Earlier work  
163 by Rossby (1999) suggests further that the well-noted annual shifting of the axis of the GS and  
164 its seasonal transport variations may result from annual variations of this “overflow” of  
165 freshwater from the north from an examination of seasonal and low frequency changes in  
166 dynamic height anomaly and transport of the GS (Sato and Rossby, 1995). Rossby (1999)  
167 speculates that such so-called “gyre interactions” may be operating on inter-annual time scales as  
168 well. Velocity observations at 52 m depth, just seaward of the shelf break along the *M/V*  
169 *Oleander* line, show a significant annual cycle of equator-ward transport with higher (lower)  
170 velocities during winter (summer) and are consistent with the GS displacement to the south by  
171 April (Rossby and Benway, 2000). IAV of the GS position shows similar behavior, with a  
172 southward displacement of the GS corresponding to time periods of higher equator-ward  
173 transport and lower SSS within both shelf and slope waters (Rossby and Benway, 2000). They  
174 suggested that since a larger volume flux along the shelf from the east into the Slope Sea must be  
175 accommodated without a significant thermocline depth increase, the GS must be displaced  
176 southward. In summary, these and other observations suggest the existence of an important  
177 upper-layer thermohaline mechanism that may partly determine the GS path over both annual  
178 and inter-annual time scales.

179 In work we present below, we examine long-term secular changes in the position of the GS  
180 “north wall” (GSNW) along with its IAV from 55° to 70° W longitude using satellite altimeter-  
181 derived data from 1993-2013 and compare our results with another published GSNW position  
182 index. We also examine long-term secular changes and IAV of upper layer LC transport and LC-  
183 related sea height variability at the shelf break in the western Labrador Sea and Grand Banks  
184 region for multi-year periods also using satellite altimeter data (following Han and Wang, 2006).  
185 Lastly, we compare the secular and inter-annual changes of LC transport with noted changes for  
186 the GSNW in both the time and frequency domains to test the thermohaline “overflow”  
187 hypothesis described above.

188

189

## 189 **Data and Methods:**

190 Merged satellite altimeter data were obtained from the Archiving Validation and  
 191 Interpretation of Satellite Oceanographic (AVISO) data center (<http://www.aviso.altimetry.fr>) for  
 192 the 21-year (1993-2013) period of record for this study. Mapped AVISO satellite altimeter data  
 193 (daily,  $\frac{1}{4}^\circ \times \frac{1}{4}^\circ$ ) were used to compute the annual mean position of the GSNW using the 50-cm  
 194 sea surface height anomaly contour measured along four longitude lines (**Fig. 1**) including  $55^\circ$ ,  
 195  $60^\circ$ ,  $65^\circ$ , and  $70^\circ$  W (Gangopadhyay *et al.*, 2016). Gridded SSH data have been used here  
 196 following Perez-Hernandez and Joyce (2014) and Gangopadhyay *et al.* (2016) to understand  
 197 IAV of the GS path, because the latitudinal excursion of the GS between  $75^\circ$  and  $55^\circ$ W ranges  
 198 between 100-300 km which is significantly larger than the error in averaging the fields from the  
 199  $\frac{1}{4}^\circ$  resolution altimeter values. We compare our method to Taylor and Stephens (1998), who  
 200 employed sea surface temperature (SST) oceanographic charts to detect the GSNW at six  
 201 longitudes from  $79^\circ$  to  $65^\circ$  W and then computed a principal component Taylor-Stephens index  
 202 (TSI) across all six longitudes for the 1966-2012 period. We note our current analysis extends  
 203 farther to the east than Taylor and Stephens (1998) but not as far to the west. Other work by  
 204 Joyce *et al.* (2000) used the location of the  $15^\circ$ C isotherm at 200-m depth to determine their GS  
 205 path index from  $75^\circ$  to  $50^\circ$  W for the 1954-1989 period, thus bracketing our study longitudes. A  
 206 recent study by Perez-Hernandez and Joyce (2014) used altimeter-derived monthly sea level  
 207 anomalies determined along 16 points between  $72^\circ$  to  $52^\circ$  W to examine GS path changes.

208 Along-track AVISO satellite altimeter data were used to estimate annual mean LC  
 209 transport across four outer-shelf altimeter track segments surrounding the Grand Banks (**Fig. 1**)  
 210 after addition of model mean values computed using linear finite element solutions that excluded  
 211 the Ekman surface current as described by Han and Wang (2006). The four segments cross the  
 212 LC at nearly perpendicular angles (Han, 2006; Han *et al.*, 2014): track 191NE in the  
 213 southwestern Labrador Sea, track 048 along the southeastern Grand Banks, track 226 at the  
 214 TGB, and track 191SW along the southwestern Grand Banks near  $52^\circ$  W ([http://www.meds-](http://www.medsdmm.dfo-mpo.gc.ca/isdm-gdsi/azmp-pmza/climat/labrador/transport-eng.htm)  
 215 [sdmm.dfo-mpo.gc.ca/isdm-gdsi/azmp-pmza/climat/labrador/transport-eng.htm](http://www.medsdmm.dfo-mpo.gc.ca/isdm-gdsi/azmp-pmza/climat/labrador/transport-eng.htm)). The lengths of  
 216 the altimeter sections were based upon the width of the mean LC at each location (Han, 2006). A  
 217 fifth altimeter track segment, track 250, extends northeastward across Hamilton Bank (**Figs. 1**)  
 218 and was used to compute a separate LC index upstream of the Grand Banks from sea height  
 219 differences measured along-track between  $54^\circ$ N and  $56.5^\circ$ N. All along-track 250 passes were  
 220 annually averaged for each year to compute the LC sea height index for the 1995-2010 time  
 221 period. In summary, satellite altimeter data were used to examine the GSNW position, LC  
 222 transport, and LC sea height changes for this study.

223 Spectral analyses of the relatively short, 21-year (1993-2013) GSNW and LC time series  
 224 required use of an autoregressive (AR) modeling technique (Gangopadhyay *et al.*, 2016). The  
 225 AR spectral method has been shown to provide superior performance for short time series  
 226 (Gangopadhyay *et al.*, 1989). Each time series had the mean and trend subtracted, and  
 227 normalized by their respective standard deviation prior to analysis using a sixth-order AR model;  
 228 the order was chosen based on our experience of similar length time-series analyses  
 229 (Gangopadhyay *et al.*, 1989 (see Case study V, Fig. 5) ; Gangopadhyay *et al.*, 2016). The  
 230 confidence interval for spectral estimates by the AR methodology is based on approximate  
 231 statistics (Kay, 1988) and remains constant across each spectrum because of the form of  
 232 variance.

233

234

234 **Results:**

235 *Gulf Stream North Wall (GSNW) Analysis*

236 Each of the four GSNW annual mean position time series for the 1993-2013 period of  
 237 record is shown along with its corresponding linear trend (Fig. 2). IAV of the GSNW position  
 238 decreases westward from 55° to 70° W, along with the magnitude of the linear trend fitted to  
 239 the data at each of the four longitudes that were analyzed (Table 1). A maximum linear  
 240 southward secular trend of  $-0.10^{\circ} \text{ y}^{-1}$  or  $-11.08 \text{ km y}^{-1}$  was measured at 55° W, decreasing  
 241 westward to a small but insignificant trend at 70° W. While only the GSNW time series trend  
 242 from 55°W (Fig. 2) displays a statistical significance of better than 95%, the significance at 60°  
 243 and 65° W are just slightly lower at approximately 88%. Therefore, the tendency for both IAV  
 244 and the magnitude of the computed (negative) trends to decrease rapidly in a westward  
 245 direction is readily apparent. Thus, the computed secular trends signal a consistent southward  
 246 movement of the GSNW between 55° and 65° W over the 21-year (1993-2013) period of  
 247 record. We note again the lack of any trend of the GSNW at 70° W (Fig. 2), in agreement with  
 248 Rossby *et al.*, (2014) who found an insignificant long-term decrease in GS layer transport near  
 249 70° W along the *M/V Oleander* transect for a nearly identical 21-year period (1992-2012).  
 250 However, additional analysis of the same data show weakening of the flux along the entire *M/V*  
 251 *Oleander* transect in agreement with a weakening AMOC (Ezer, 2015). The co-variation of  
 252 high (low) transport and northward (southward) position of the GS eastward of Cape Hatteras  
 253 is supported by earlier modeling work by Chaudhuri *et al.* (2011).

254 Subtraction of the secular trend of GSNW movement for each of the time series located  
 255 at 55°, 60°, 65°, and 70° W, results in time series of IAV of GSNW position residuals at each  
 256 longitude. Comparisons between GSNW residuals (Fig. 3a, Table 1) show that the largest  
 257 values consistently occur along eastern-most longitudes at 55° W (rms  $1.13^{\circ}$ ) and at 60° W  
 258 (rms  $0.60^{\circ}$ ) with much-reduced values along western-most longitudes at 65° W (rms  $0.31^{\circ}$ ) and  
 259 70° W (rms  $0.24^{\circ}$ ). Furthermore, GSNW residuals at all four longitudes clearly show shorter  
 260 period fluctuations and appear out-of-phase prior to 2003, with longer period fluctuations  
 261 beginning during 2003 that appear largely in-phase across all four longitudes (Fig. 3a).  
 262 Corresponding AR power spectra for GSNW residual time series at 55°, 60°, and 65° W  
 263 clearly show both the shorter period ( $\sim 2.5$  year) and longer period ( $\sim 5$  year) fluctuation peaks  
 264 (Fig. 3b) readily apparent in the time series. GSNW power spectra at 65° and 70° W show  
 265 additional longer period peaks at  $\sim 10$  years and  $\sim 7$  years, respectively, with both an absence of  
 266 the  $\sim 5$  year peak and a shift of the shorter period peak to near  $\sim 3.5$  years at 70° W (Fig. 3b).

267  
 268 *Labrador Current (LC) Analysis*

269 Annual mean along-stream LC transport time series for the 1993-2013 period of record  
 270 measured across two outer-shelf altimeter track segments show highly significant decreasing  
 271 linear trends of about  $-0.5 \text{ Sv}$  per decade north of Flemish Pass (191NE) and along the eastern  
 272 flank of the Grand Banks (048) (Fig. 4, Table 1). Further downstream, the trend of LC transport  
 273 time series along track segment 226 near the TGB, while still decreasing ( $-0.2 \text{ Sv}$  per decade), is  
 274 not highly significant. However, the trend of LC transport time series for segment 191SW near  
 275 52° W along the southwestern flank of the Grand Banks increases at about  $+0.4 \text{ Sv}$  per decade  
 276 with somewhat higher significance (Fig. 4, Table 1).

277  
 278

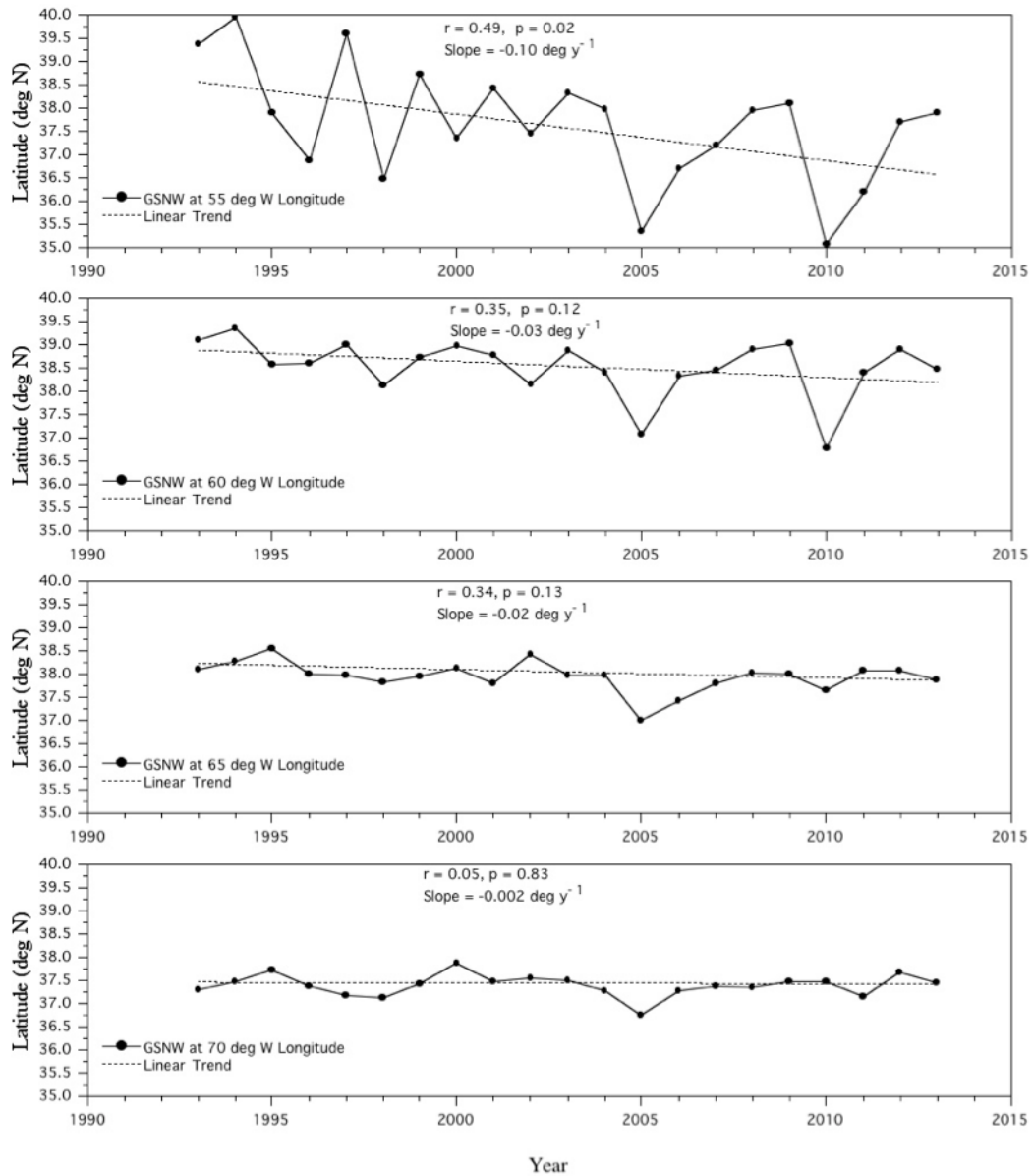


Figure 2. Annual mean latitude of the GSNW position computed along 55°, 60°, 65°, and 70° W from AVISO mapped altimeter data from 1993-2013, along with computed linear trends.

After removal of linear trends, IAV of LC transport residuals (Fig. 3a, Table 1) is large along downstream segments 226 near the TGB (rms 1.02 Sv), and 191SW near 52° W along the southwestern Grand Banks (rms 1.05 Sv). IAV is much reduced further upstream along segments 048 (rms 0.41 Sv) and 191NE (rms 0.29 Sv) along the eastern Grand Banks and north of Flemish Pass, respectively (Fig. 3a, Table 1). In addition, reduced-magnitude LC transport residuals along upstream segments 191NE and 048 appear to be in phase over most of the 21-year period of record, while the much larger residuals along downstream segments 226 and 191SW appear to be largely out-of-phase for the same period (Fig. 3a).

**Table 1. Statistics of GSNW and LC Secular Trends and Inter-Annual Residuals**Significant correlation values ( $p \leq 0.05$ ) are shown in bold.

N = 21 for all statistics shown.

<b>GSNW Longitude</b>	<b>Y-intercept (<math>^{\circ}</math> N), Slope (<math>^{\circ}</math> Lat <math>y^{-1}</math>) Residual rms (<math>^{\circ}</math> Lat)</b>	<b>r (p-value)</b>
55 $^{\circ}$ W	38.16, -0.10 1.13	<b>-0.49</b> <b>(0.02)</b>
60 $^{\circ}$ W	38.87, -0.03 0.60	-0.35 (0.12)
65 $^{\circ}$ W	38.22, -0.02 0.31	-0.34 (0.13)
70 $^{\circ}$ W	37.45, 0.00 0.24	-0.05 (0.83)
<b>LC Altimeter Segment</b>	<b>Y-intercept (Sv), Slope (Sv <math>y^{-1}</math>) Residual rms (Sv)</b>	<b>r (p-value)</b>
191NE	6.55, -0.05 0.29	<b>-0.74</b> <b>(0.001)</b>
048	2.89, -0.05 0.41	<b>-0.65</b> <b>(0.001)</b>
226	1.80, -0.02 1.02	-0.10 (0.65)
191SW	0.64, 0.04 1.05	+0.22 (0.35)

Corresponding AR power spectra of LC transport residuals along upstream altimeter track segment 191NE, just north of Flemish pass, and downstream segments 226 at the TGB and 191SW near 52 $^{\circ}$  W on the southwestern flank of the Grand Banks show both shorter period ( $\sim 3$  year) and longer period ( $\sim 6-8$  years) peaks (Fig. 3b). Upstream segment 048 located along the

370 eastern flank of the Grand Banks only shows the longer period peak (~8 years), with no evidence  
 371 of the shorter period (~3 year) peak (Fig. 3b). Three of the eastern GSNW locations (65°W,  
 372 60°W and 55° W) peak at 5 years, while the southward flowing LC transport (across 191NE)  
 373 shows a distinct 6-year peak (Fig. 3b). A number of GS and LC locations show peaks in the 2-to-  
 374 3-year range. While these are individually significant, a coherence analysis could not be  
 375 performed due to lack of degrees of freedom for the cross spectra for these short time-series.  
 376 Note that these two periods (2-3 years, 5-6 years) also coincide with the characteristic periods for  
 377 the atmospheric NAO forcing described by Gangopadhyay *et al.* (2016).

378

### 379 **Discussion:**

380

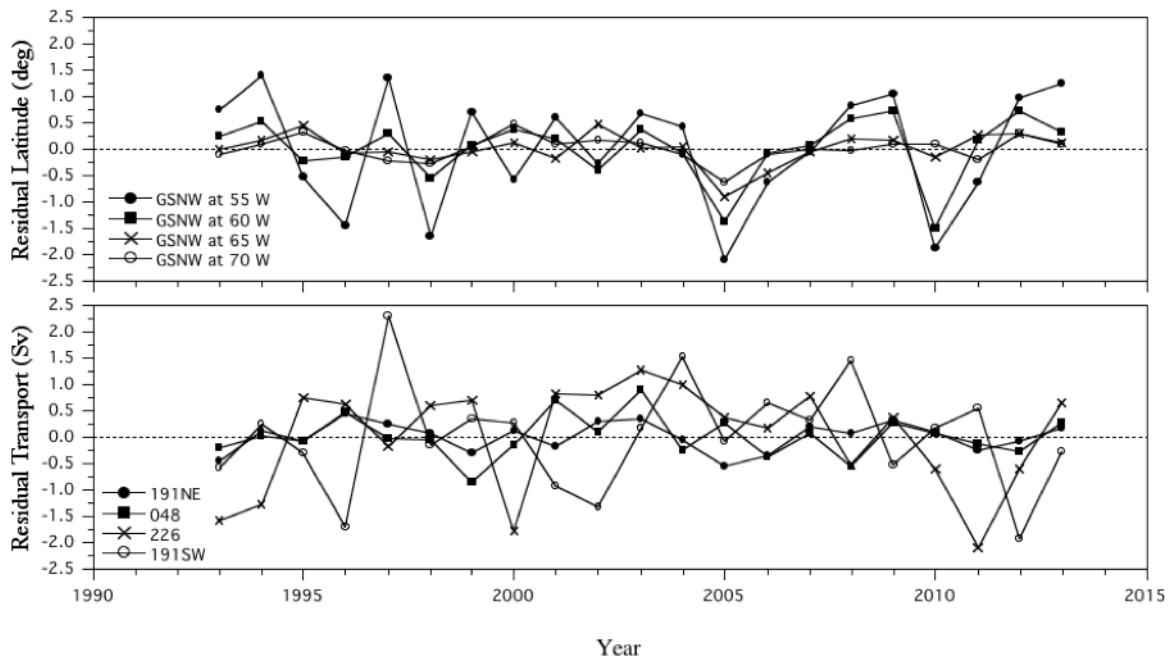
#### 381 *Combined Gulf Stream North Wall (GSNW) and Labrador Current (LC) Analysis*

382

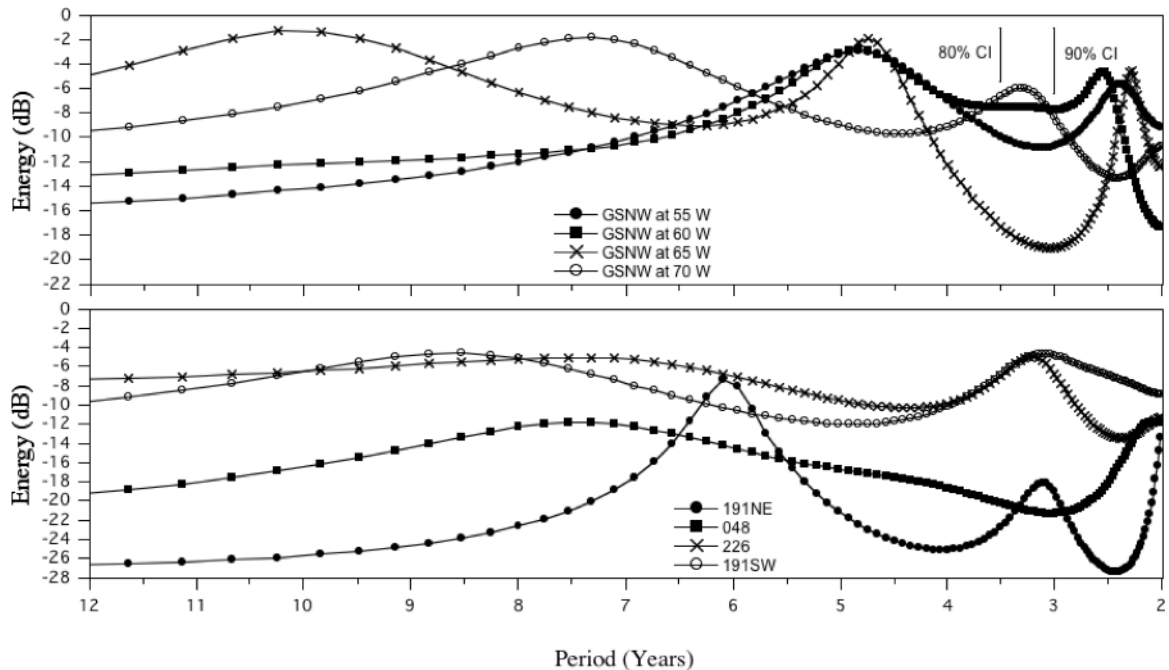
383 Inter-comparison of our GSNW position and LC transport time series allows the covariance  
 384 of secular trends and IAV of the two western boundary currents to be examined in both the time  
 385 and frequency domains. Subsequently, we also expand on a simplified test of the thermohaline  
 386 “overflow” hypothesis described above using some basic assumptions and a simplified volume  
 387 calculation methodology (Rossby, 1999; Rossby and Benway, 2000).

388 GSNW results from this study show a consistent long-term southward-directed secular  
 389 trend for the GSNW at all four study longitudes that decreases westward from 55° to 70° W with  
 390 a maximum (minimum) southward secular movement of approximately 220 km (4 km) at 55° W  
 391 (70° W) for the 21-year (1993-2013) study period. However, although our results are in  
 392 agreement with the southward shift reported by Ezer *et al.* (2013) between 70° and 74° W, they  
 393 observed a northward shift between 68° and 70° W, showing that long-term shifts of the GS can  
 394 be complex. Nevertheless, the large east-to-west difference in the secular movement of the  
 395 GSNW over the two decades of this study suggests a mechanism that is maximal in the eastern  
 396 portion of our study domain (near 55° W) such as southward LC transport. Other mechanisms,  
 397 e.g., changes over the sub-tropical gyre may be important farther to the west (See Fig. 4 in Ezer,  
 398 2015). Interestingly, studies have shown that annual shifts of the GSNW are also maximal (~70  
 399 km) farthest east, near 63° W (secondary maximum of 30 km near 67° W) but are much smaller  
 400 west of 70° W, using eight years of satellite-derived infrared SST imagery (Lee and Cornillon,  
 401 1995). In a recent study, Perez-Hernandez and Joyce (2014) show from monthly sea level  
 402 anomalies that the leading mode of IAV of GS position are meridional shifts of approximately  
 403 100 km using their 16-point index, with higher modes representing GS meandering that vary  
 404 with GS strength (Kelly *et al.*, 2010). Their typical meridional shift of 100 km compares  
 405 favorably with our mean RMS value of approximately 63 km computed as the average of the  
 406 four RMS values shown in Table 1 after conversion to kilometers. Comparison of their highly-  
 407 resolved monthly GS position time series with our annual mean GSNW position residuals shows  
 408 some agreement, with extreme northward (southward) excursions during 1994-1995, 2000,  
 409 2006-2008, 2012 (1996, 1998, 2005, 2010). Similarly, GSNW path variability from this analysis  
 410 at 65° and 70° W (Figs. 2 & 3a top panel) also shows agreement with the GS position determined  
 411 along the *M/V Oleander* line as shown in Figure 3c by Ezer (2015). In addition, extreme  
 412 southward GS excursions shown for 2005 and 2010 (Fig. 2 & 3a top panel) also coincide with  
 413 extreme negative NAO states for those years, with 2010 corresponding to the period of weak  
 414 AMOC noted in other studies (McCarthy *et al.*, 2012; Ezer, 2015; Goddard *et al.*, 2015)

415



433 Figure 3a. (Top Panel) Annual mean GSNW position residuals along 55°, 60°, 65°, and 70° W  
 434 from AVISO mapped altimeter data from 1993-2013, after subtraction of computed linear trends.  
 435 (Bottom Panel) Annual mean Labrador Current transport residuals computed along outer-shelf  
 436 altimeter track segments 191NE, 048, 226, and 191SW from AVISO along-track altimeter data  
 437 from 1993-2013, after subtraction of linear trends.



457 Figure 3b. (Top Panel) Normalized AR power spectra (order 6) of GSNW position residual time  
 458 series from 55°, 60°, 65°, and 70° W in Fig. 3a above. (Bottom Panel) Normalized AR power  
 459 spectra (order 6) of Labrador Current transport residual time series shown for altimeter track  
 460 segments (191NE, 048, 226, and 191SW) in Fig. 3a above. Also shown are the 80% and 90%  
 461 spectral confidence intervals (CI).

462 A recent study shows that during the last decade, SST in the Gulf of Maine (GOM) has  
463 increased at a rate faster than 99% of the global oceans (Pershing *et al.*, 2015) and partially  
464 attributes this warming to a northward excursion of the GS, along with changes in both the  
465 Atlantic Multi-decadal Oscillation and Pacific Decadal Oscillation. Furthermore, they suggest  
466 that such changes may be partly responsible for the collapse of the cod fishery in New England  
467 waters, including the GOM. However, as shown in our analysis, the GSNW displays a clear  
468 southward trend over the past two decades at 55°, 60°, and 65° W, although displaying recent  
469 (2012-2013) large northward-directed residuals following the extreme southward GSNW  
470 position residuals for 2010 (Figs. 2 & 3a top panel). Specifically, while the long-term (21 years)  
471 southward trend at 70°W is not significant; it is significant at 85% or more at both 65° and  
472 60°W. From 2005-2013 (period of study by Pershing *et al.* (2015)) our analysis does show a  
473 small northward trend in the GSNW at 70°W and 65°W, due largely to the extreme southward  
474 excursion of 2005, small northward shift during 2006-2009, southward movement for 2010  
475 (65°W) or 2011 (70°W), followed by northward movement for 2012 (Fig. 2). In contrast, the  
476 eastern GS region at 60° and 55°W exhibits a clear periodicity of five years added to the  
477 significant long-term southward trend-line from 2005-2013 (Fig. 2). In any case, shelf SST north  
478 of Cape Hatteras, including the GOM, is warming at between 1.8-2.5 times faster than regional  
479 atmospheric trends and is thus similar to atmospheric trends over Labrador and the Arctic,  
480 supporting advection from the north (Shearman and Lentz, 2010), with noted sub-surface  
481 warming as well along the *M/V Oleander* expendable bathythermograph transect between 1977-  
482 2013 (Forsyth *et al.*, 2015).

483 An examination of LC transport trends for the same 21-year (1993-2013) study period  
484 shows that they differ markedly from north-to-south along segments 191NE, 048, 226 and  
485 191SW, with trends that transition from strongly negative in the north (191NE and 048) to  
486 positive in the south (191SW) on the southwestern flank of the Grand Banks in agreement with  
487 an analysis of data from some of the same altimeter sections (Han *et al.*, 2014). Both our long-  
488 term secular analysis and the earlier trend analysis by Han *et al.*, (2014) show that the LC  
489 transport off the northeastern Newfoundland slope is out-of-phase with that over the Scotian  
490 slope for nearly identical ~20-year periods of record. In addition, the increasing trend computed  
491 for segment 191SW near 52° W from our study (Fig. 4, Table 1) agrees with LC transport from  
492 segment 176 near 61° W off the central Scotian shelf (not shown) reported by Han *et al.*, (2014).  
493 Furthermore, results from Han *et al.*, (2014) also show that LC transport over the Newfoundland  
494 slope (Scotian slope) is positively (negatively) correlated with the winter North Atlantic  
495 Oscillation (NAO) index for inter-annual through decadal time scales, with the Grand Banks  
496 being a region of transition.

497 A shelf-wide near-surface salinity analysis (Bisagni, 2016) shows that large inter-annual  
498 anomalies are ubiquitous along the entire eastern seaboard of both the United States' and  
499 Canada's continental shelf, with strong variability located west of the TGB between 1973-2013.  
500 The same analysis shows near-surface salinity anomaly magnitudes increasing steadily from the  
501 Eastern Scotian Shelf to the DelMarVa/Hatteras shelf over a distance of ~1400 km and are  
502 synchronous (coherent at 0-year lag). These observations suggest that an along-shelf, wind-  
503 modulated, flux-variation model (Sundby and Drinkwater, 2007; Li *et al.*, 2014), i.e., a varying  
504 flux across the mean along-shelf salinity gradient, as the most likely mechanism (Bisagni, 2016).  
505 In addition, *M/V Oleander* SSS data across the Middle Atlantic Bight region from New Jersey to  
506 Bermuda over a 21-year period (1978-1998) show synchronous salinity anomalies extending  
507 across both the shelf and Slope Sea regions (Rossby and Benway, 2000) also supporting large-  
508

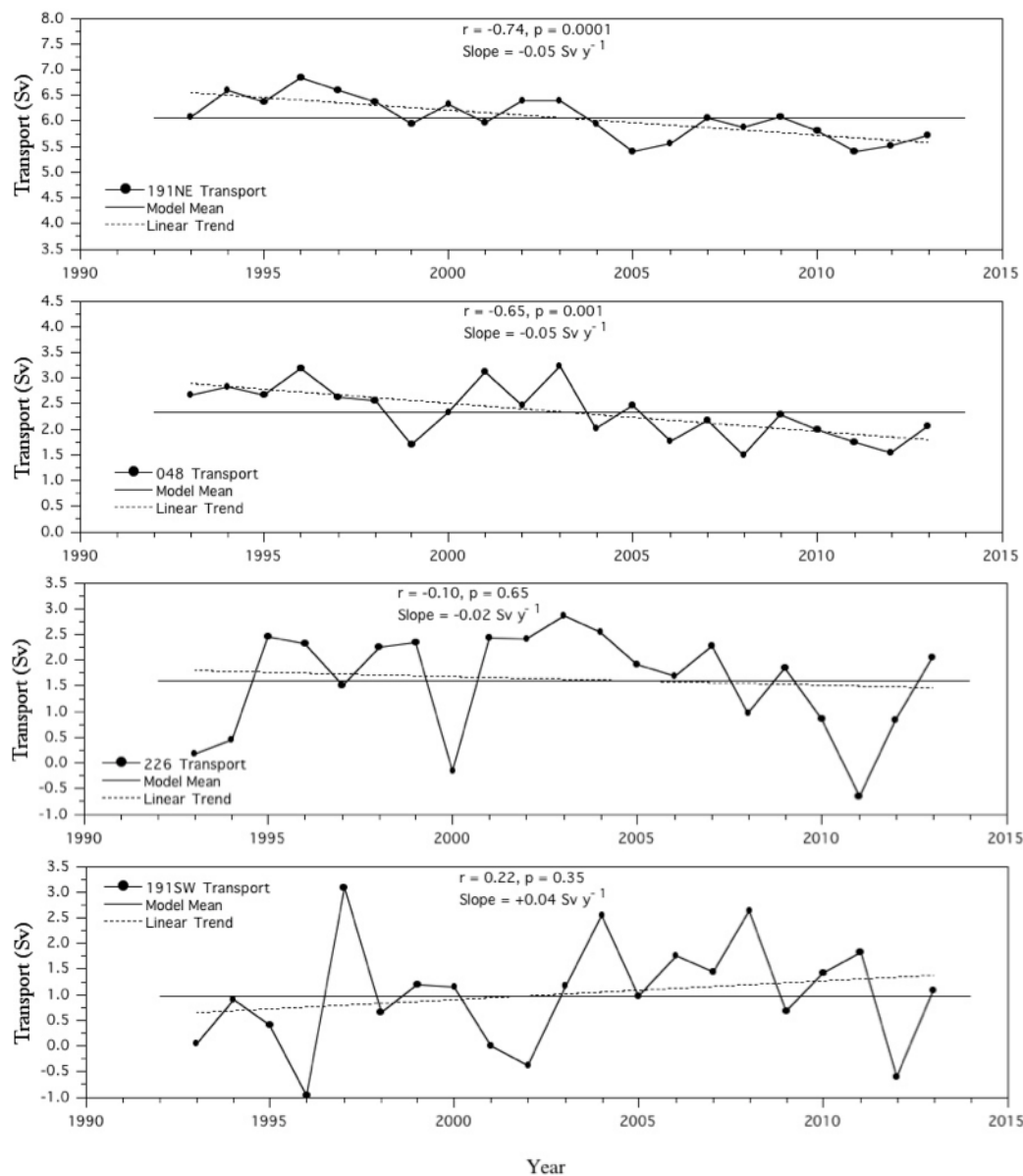


Figure 4. Annual mean Labrador Current transport computed across four outer-shelf altimeter track segments (191NE, 048, 226, and 191SW) shown in Figure 1 from AVISO along-track altimeter data from 1993-2013, along with the regression model mean across each segment, and computed linear trends. Positive (+) values signify equator-ward transport.

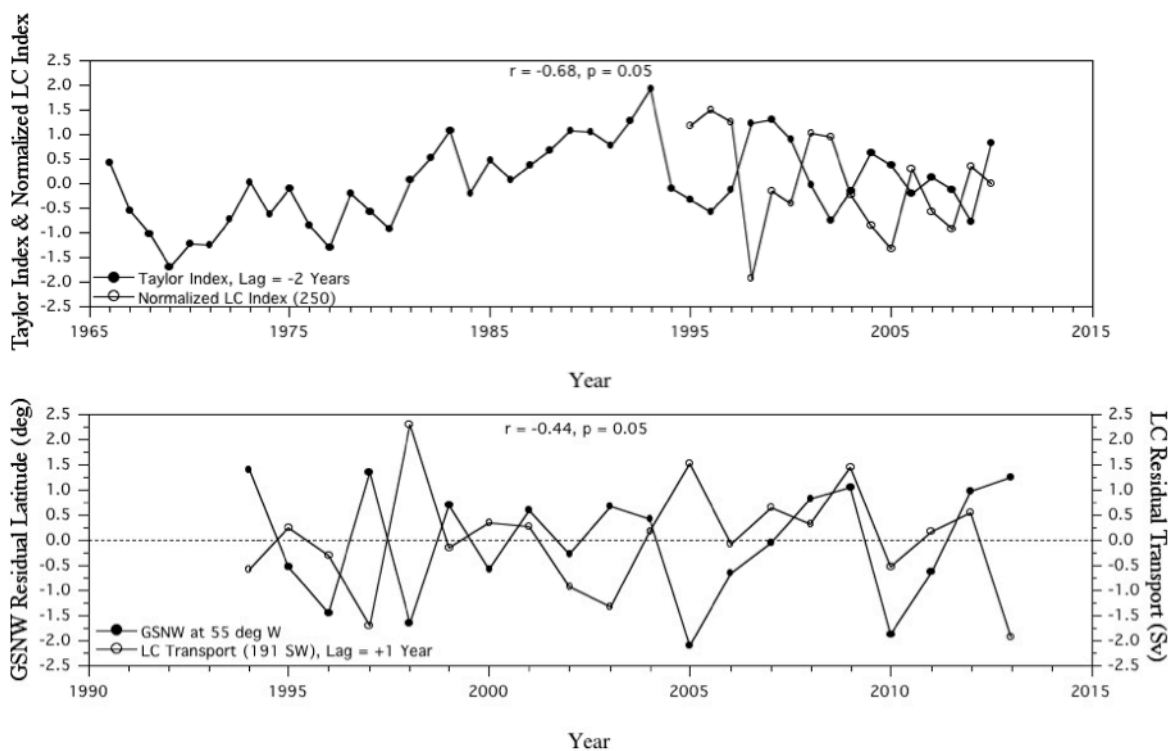
scale flux and temperature variations that may extend into the Slope Sea as discussed for slope water velocity anomalies (Peña-Molino and Joyce, 2008).

IAV of LC transport at the shelf break along segment 191SW near 52° W from this study is large (Fig. 4), with a strong negative (positive) transport anomaly corresponding to strong positive (negative) salinity anomalies as shown by other studies for 1996 and 1997, (Rossby and Benway, 2000; Flagg *et al.*, 2006; Bisagni, 2016). Sea surface height along ground track segment 250 is chosen as representative of upstream LC transport within the Labrador Sea. This new upstream LC index is constructed along segment 250 between 54° and 56.5° N, using both ERS-

587 2 and ENVISAT satellite missions, with the general structure of the SSH along this segment  
 588 being high to low SSH going in the offshore direction (towards higher latitudes), consistent with  
 589 the Labrador Current flow at this location (Fig. 1). The LC index is computed from the height  
 590 difference between 54° N and 56.5° N from each 250 pass and then annually averaged for the  
 591 1995 to 2010 time period.

592 Results from a comparison between annual TSI values with the more distal upstream  
 593 segment 250 LC index within the Labrador Sea from 1995-2010 show the “broad scale” TSI of  
 594 GS position to be highly correlated with the LC index ( $r=-0.68$ , significant at 95% level), with  
 595 the LC index leading the TSI by 2 years (Fig. 5, top panel). More specifically, the LC index  
 596 shows high values for 1996, 2001, 2006, and 2009 followed two years later by low TSI values;  
 597 signifying that increases in our LC index along segment 250 are followed two years later by  
 598 southward shifts in GS position. Similarly, lower values of our LC index observed for 1998,  
 599 2005, and 2008 are followed two years later by northward shifts in GS position (as represented  
 600 by the TSI). The anomalously high LC index for 1996, high transport to the south, has been  
 601 previously described as the strong LC ‘pulse’ in previous studies (e.g., Han, 2006). Farther to the  
 602 south and near the TGB, comparison of the GSNW position residuals at 55° W with the  
 603 downstream LC transport residuals along segment 191SW near 52° W at 0-year lag (not shown)  
 604 does not show a significant relationship between the two signals ( $r = 0.18$ ,  $p = 0.43$ ). However,  
 605 when the LC residual signal is lagged by +1 year (Fig. 5, lower panel), a significant negative  
 606 correlation results ( $r = -0.44$ ,  $p = 0.05$ ), meaning that the previous year’s LC transport residual  
 607 near 52° W is related to the current year’s GSNW position residual at 55° W, similar to the  
 608 maximum 12 month (1-year) lag reported by Peña-Molino and Joyce (2008) for the relationship  
 609 between cooler (warmer) slope water SST anomalies and more-southerly (northerly) shifts of the  
 610 GS. A 1-year delay for the effect of changes in annual mean LC transport near 52° W on the  
 611 GSNW position at 55° W does not seem unreasonable given the 2-year delay we find between  
 612 the more-distal upstream segment 250 LC index and the broad scale TSI. This 1-year delay is in  
 613 agreement with the 1-year delay reported earlier related to the Icelandic Low (Sanchez-Franks *et*  
 614 *al.*, 2016). Lastly, a significant correlation ( $r = 0.48$ ,  $p \leq 0.05$ ) was computed between the nearly  
 615 contiguous *M/V Oleander*-derived southward-directed slope current (a LC extension)  
 616 fluctuations and GS position values at 0-year lag for 1993-2012 (Ezer, 2015), and supports our  
 617 correlation results near 52° W after consideration of the sign conventions used for each analysis.

618 A recent study by Gangopadhyay *et al.*, (2016) has shown that the GS has behaved  
 619 differently along its path from 75° W to 55° W over the last four decades. Specifically, the  
 620 GSNW latitudinal excursion variability west of 60° W, exhibits a dominant time scale of 8-10  
 621 years, while eastward from 65° W, a 4-5 year time scale was also present, with a 2.5-3.5 year  
 622 time scale being present at all four longitudes from this study (Figs. 3a and 3b). The 8-10 year  
 623 time scale present from 70° W to 65° W is clearly related to the NAO signal as shown by other  
 624 investigators (Cook *et al.*, 1998; Wunsch, 1999) and also GS intensity and coastal sea level (Ezer  
 625 *et al.*, 2013). We can also speculate further that both the 4-5 year and the 2.5-3.5 year IAV may  
 626 also be related to the NAO due to possible interactions between the NAO and the LC as  
 627 described by Han *et al.* (2014), caused by variations in the strength and location of the Icelandic  
 628 Low for a lag of +1 year (Sanchez-Franks *et al.*, 2016). The co-plot of the GSNW residual time  
 629 series at 55° W with the LC residual time series along segment 191SW near 52° W does show a  
 630 significant relationship between the two signals when the LC residual signal is lagged by +1  
 631 year, i.e., changes in the LC transport near 52° W lead the GSNW position changes by one year  
 632 (Fig. 5, lower panel).



650

660

662

663

664 Figure 5 (Top Panel) Annual mean TSI (-2-year lag) along with annual mean LC index for pass  
 665 250 in the Labrador Sea from Fig. 1. Correlation coefficient and p-value ( $n = 16$ ) for TSI at -2-  
 666 year lag. Note that the -2-year lag applied to the TSI as shown above is equivalent to a +2-year  
 667 lag applied to the LC index as described in the text. (Bottom Panel) Annual mean GSNW  
 668 position residuals along  $55^\circ$  W along with annual mean LC transport residuals (+1-year lag)  
 669 computed along segment 191SW near  $52^\circ$  W. Correlation coefficient and p-value ( $n = 20$ ) for  
 670 LC at +1-year lag.

671

672 *A Possible Model*

673

674 A volume flux calculation by Rossby (1999) was used to estimate the annual movement of  
 675 the GSNW along the southern boundary of the Slope Sea due to a hypothesized annual baroclinic  
 676 transport cycle of 0.5 Sv across the shelf-slope front, i.e., a “spilling” of less-saline waters into  
 677 the Slope Sea from the shelf. Assuming no change in the depth of the Slope Sea upper layer (200  
 678 m), the volume flux calculation resulted in an annual GS movement of 42 km, a number that is  
 679 midway between the two maximum annual values reported using satellite-derived SST data by  
 680 Lee and Cornillon (1995). Alternatively, the annual baroclinic transport could also have been  
 681 accommodated by an increase in Slope Sea upper layer depth of 29 m. Rossby (1999) further  
 682 describes how both the annual cycle in the position of the GS, i.e., north during fall and south  
 683 during spring (Iselin, 1940; Watts, 1983) and the 8 Sv annual cycle in GS transport (maximal  
 684 during early summer as reported by Sato and Rossby (1995)) may be related to the June timing  
 685 of the maximum difference in the Fofonoff potential energy anomaly (PEA) values. Rossby’s  
 686 hypothesis is based upon changes in layer depth across the GS measured from the Slope Sea to  
 687 the Sargasso Sea resulting in the annual GS cycles described above (Sato and Rossby, 1995).

688 We extended the volume flux calculation methodology described by Rossby (1999),  
689 assuming a simplified length and depth (2000 km × 200 m) for the Slope Sea located north of the  
690 GS. Integrating the calculated positive long-term trend of LC transport into the Slope Sea at 52°  
691 W (segment 191SW) over the 1993-2013 period (Table 1), we can account for 68.4% (0.53°  
692 latitude) of the mean southward-directed secular shift of the GSNW (0.77° latitude) averaged  
693 across all four GSNW longitudes used herein. A second volume flux calculation using the  
694 measured inter-annual LC rms residual of +1.04 Sv at 52° W integrated over one year results in a  
695 corresponding southward residual for the GSNW of 79 km, or 63% of the observed 125.6 km  
696 (1.13°) GSNW rms residual at 55° W. We speculate that the remaining 37% of the unexplained  
697 GSNW rms residual may result from IAV of shelf water volume (Mountain, 2003) and position  
698 of the shelf-slope front separating shelf and slope waters (Bisagni *et al.*, 2009).

699 In summary, our secular and inter-annual volume flux calculations using measured LC  
700 transport numbers, although crude, result in plausible secular and inter-annual GSNW fluctuation  
701 magnitudes. This level of agreement supports direct interaction between the upper layers of the  
702 sub-polar and sub-tropical gyres within the North Atlantic over secular and inter-annual time  
703 scales as suggested by Rossby (1999) and Rossby and Benway (2000). However, the proposed  
704 simple volume flux mechanism, although plausible, should be compared with future long-term  
705 analyses of computed Fofonoff PEA values in both the Slope Sea and Sargasso Sea as computed  
706 by Sato and Rossby (1995) in their dynamical analysis. While the secular and inter-annual time  
707 scales of GSNW variability are most likely due to NAO modulation of the North Atlantic  
708 circulation including LC transport as suggested by Marshall *et al.*, (2001), this study shows that  
709 additional research is needed to confirm the actual dynamical mechanism related to gyre  
710 interactions. Important needs are much longer records of GSNW positions and LC transports to  
711 determine if the southward secular trend of the GSNW observed from 1993-2013 will continue  
712 and if these changes are related to variations in LC transport from the north.

713  
714  
715  
716  
717  
718  
719  
720  
721  
722  
723  
724  
725  
726  
727  
728  
729  
730  
731  
732  
733

### 733 **Summary and Conclusions:**

734 Recent work has shown that changes in the GS position after its separation from the coast  
 735 at Cape Hatteras may be a key to the understanding of changes in the AMOC, sea level  
 736 variability and coastal flooding along the eastern seaboard of North America, and recently  
 737 observed changes in coastal and offshore ecosystems. In this study we compared secular change  
 738 and IAV of the GSNW position between 55° and 70° W with equator-ward LC transport along  
 739 the southwestern Grand Banks near 52° W and a LC index in the western Labrador Sea using  
 740 approximately two decades of satellite altimeter data.

- 741 1) Results at 55°, 60°, and 65° W show a significant southward (negative) secular trend for the  
 742 GSNW, decreasing to a small but insignificant southward trend at 70° W, with IAV of de-  
 743 trended GSNW position residuals also decreasing to the west, but largely in phase, especially  
 744 from 2003-2013.
- 745 2) The long-term secular trend of annual mean upper layer (200 m) LC transport near 52° W is  
 746 positive with a transition to negative trends near the Tail of the Grand Banks (TGB) and into  
 747 the Labrador Sea along the eastern Grand Banks in agreement with previous work.
- 748 3) Secular changes we report for the GSNW and LC have occurred during the time of a  
 749 weakening AMOC over the past decade and that both past and ongoing AMOC monitoring  
 750 efforts (RAPID and OSNAP) will continue to provide a more complete picture of the total  
 751 AMOC over time.
- 752 4) IAV of the Taylor-Stephens Index (TSI) computed from the first principal component of the  
 753 GSNW position measured from 79° to 65° W shows a significant relationship with IAV of  
 754 our LC Index computed along altimeter ground track 250 located across Hamilton Bank  
 755 (north of the Grand Banks) in the western Labrador Sea from 1995-2010. Increased  
 756 (decreased) sea height differences along altimeter ground track 250 are significantly  
 757 correlated ( $r = -0.68$ ,  $p = 0.05$ ) with a more southward (northward) TSI two years later (a LC  
 758 index lag of +2-years).
- 759 5) IAV of LC transport residuals near 52° W along the southwestern Grand Banks are  
 760 significantly correlated at a lag of +1-year ( $r = -0.44$ ,  $p = 0.05$ ) with IAV of GSNW position  
 761 residuals at 55° W, with positive (negative) LC transport residuals corresponding to  
 762 southward (northward) GSNW positions, i.e., changes in the LC transport lead the GSNW  
 763 position changes by one year.
- 764 6) Spectral analysis of IAV reveals corresponding spectral peaks at 5-7 years and 2-3 years for  
 765 the North Atlantic Oscillation (NAO), GSNW (70°-55°W) and LC transport near 52° W for  
 766 the 1993-2013 period suggesting a connection between these phenomena.
- 767 7) An upper-layer (200 m) slope water volume calculation using the LC IAV rms residual of  
 768 +1.04 Sv near 52° W results in an estimated GSNW IAV position residual of 79 km, or 63%  
 769 of the observed 125.6 km (1.13°) rms value at 55° W.
- 770 8) A similar upper-layer slope water volume calculation using the positive long-term, upper-  
 771 layer LC transport trend accounts for 68% of the mean observed secular southward shift of  
 772 the GSNW between 55° and 70°W over the 1993-2013 period.
- 773 9) Our work provides additional observational evidence supporting interactions between the  
 774 upper layers of the sub-polar and sub-tropical gyres within the North Atlantic over both  
 775 secular and inter-annual time scales as suggested in previous studies. This interaction may be  
 776 in addition to and a direct result of wind-forcing supplied by changes in the NAO over the  
 777 entire North Atlantic Ocean as described by others (Marshall *et al.*, 2001; Chaudhuri *et al.*,  
 778 2011).
- 779

779 **Acknowledgements:**

780

781 This work was supported in part through a recent sabbatical (Bisagni) from the University of  
782 Massachusetts, Dartmouth, hosted by G. Gawarkiewicz at the Woods Hole Oceanographic  
783 Institution (WHOI), Woods Hole, Massachusetts. This work was also partly supported  
784 (Gangopadhyay) by NSF Grants OCE-0815679 and OCE-0535379, and NOAA Grant  
785 NA11NOS0120038 [for the implementation of the Mid-Atlantic Regional Association Coastal  
786 Ocean Observing System (MARACOOS)] during the development of some of the analyses  
787 presented herein. This work was also partly supported (Sanchez-Franks) by NSF Grant OCE-  
788 0825418. We are grateful to Dr. A. Schmidt, University of Massachusetts, Dartmouth, for  
789 providing the Gulf Stream North Wall position data, to Dr. G. Han, Northwest Atlantic Fisheries  
790 Centre, Fisheries and Oceans Canada, St. John's, Newfoundland, for providing the Labrador  
791 Current transport data, and to five anonymous reviewers for their thoughtful comments and  
792 suggestions. AS-F thanks C. N. Flagg, H. T. Rossby and K. A. Donohue for feedback and  
793 comments on the Labrador Current and Gulf Stream interaction part of the analysis.

794

795

796

796 **References:**

797

- 798 Andres, M., Gawarkiewicz, G. G. & Toole, J. M. Interannual sea level variability in the western  
799 North Atlantic: Regional forcing and remote response. *Geophys. Res. Lett.*, **40**, 5915-5919,  
800 doi: 10.1002/2013GL058013 (2013)
- 801 Bisagni, J. J., Kim, H-S., & Chaudhuri, A. Inter-annual variability of the shelf slope front  
802 position between 75° and 50° W. *J. Mar. Syst.*, doi:10.1016/j.jmarsys.2008.11.020 (2009)
- 803 Bisagni, J. J. Salinity variability along the eastern continental shelf of Canada and the United  
804 States, 1973-2013. *Cont. Shelf Res.* **126**, 89-109 (2016)
- 805 Boon, J. D. Evidence of sea level acceleration at U.S. and Canadian tide stations, Atlantic Coast,  
806 North America. *J. Coastal Res.* **28**, 1437-1445 (2012)
- 807 Chaudhuri, A. H., Gangopadhyay, A., & Bisagni, J. J. Response of the western North Atlantic  
808 basin to characteristic high and low phases of the North Atlantic Oscillation. *Ocean*  
809 *Modell.* **39**, 220-232 (2011)
- 810 Cook, E. R., D'Arrigo, R. D., & Briffa, K. R. The North Atlantic Oscillation and its expression  
811 in circum-Atlantic tree-ring chronologies from North America and Europe. *Holocene*, **8**, 9-  
812 17 (1998)
- 813 Ezer, T. & Corlett, W. B. Is sea level rise accelerating in the Chesapeake Bay? A demonstration  
814 of a novel new approach for analyzing sea level data. *Geophys. Res. Lett.* **39**, L19605  
815 (2012)
- 816 Ezer, T., Atkinson, L. P., Corlett, W. B. & Blanco, J. L. Gulf Stream's induced sea level rise and  
817 variability along the U.S. mid-Atlantic coast. *J. Geophys. Res.* **118**, 685-697 (2013)
- 818 Ezer T. & Atkinson L. P., Accelerated flooding along the U.S. East Coast: On the impact of sea-  
819 level rise, tides, storms, the Gulf Stream, and the North Atlantic Oscillations. *Earth's*  
820 *Future* **2(8)**:362-382. doi: 10.1002/2014EF000252, (2014)  
821
- 822 Ezer, T., Detecting changes in the transport of the Gulf Stream and the Atlantic overturning  
823 circulation from coastal sea level data: The extreme decline in 2009-2010 and estimated  
824 variations for 1935-2012, *Glob. Planet. Change*, **129**, 23-36,  
825 doi:10.1016/j.gloplacha.2015.03.002, (2015).  
826
- 827 Flagg, C. N, Dunn, M., Wang, D-P, Rossby, H. T., & Benway, R. L. A study of the currents of  
828 the outer shelf and upper slope from a decade of shipboard ADCP observations in the  
829 Middle Atlantic Bight. *J. Geophys. Res.* **111** , C06003, doi:10.1029/2005JC003116 (2006)
- 830 Forsyth, J. S. T., Andres, M. & Gawarkiewicz, G. G. Recent accelerated warming of the  
831 continental shelf off New Jersey: Observations from the *CMV Oleander* expendable  
832 bathythermograph line. *J. Geophys. Res.* **120** , doi:10.1002/2014JC010516 (2015)

- 833 Gangopadhyay, A., Cornillon, P. & Jackson, L. B. Autoregressive modeling for spectral analysis  
834 of oceanographic data. *J. Geophys. Res.* **94**, 16215–16226 (1989)
- 835 Gangopadhyay, A., Chaudhuri, A. H., & Taylor, A. H. On the nature of temporal variability of  
836 the Gulf Stream Path from 75° to 55°W. *Earth Interact.* **20**, (9) 17 pp. (2016)
- 837 Goddard P. B., Yin J., Griffies S. M., Zhang S., An extreme event of sea-level rise along the  
838 Northeast coast of North America in 2009–2010. *Nature Comm.* **6**  
839 doi:10.1038/ncomms7346 (2015)  
840
- 841 Han, G. Low-frequency variability of sea level and currents off Newfoundland. *Adv. Space Res.*  
842 **38**, 2141-2161 (2006)  
843
- 844 Han G. & Wang Z. Monthly-mean circulation in the Flemish Cap region: a modeling study,  
845 *Estuar. Coastal Model.*, ASCE, 138-154, (2006)  
846
- 847 Han, G., Chen, N. & Ma, Z. Is there a north-south phase shift in the surface Labrador Current  
848 transport on the interannual-to-decadal scale? *J. Geophys. Res.* **119**, 276-287 (2014)
- 849 Iselin, C. O. D. Preliminary report on long period variations in the transport of the Gulf Stream  
850 system. *Pap. Phys. Oceanogr. and Meteor.* **8**(1), 40 (1940)
- 851 Joyce, T. M., Deser, C., & Spall, M. A. The relation between decadal variability of subtropical  
852 mode water and the North Atlantic Oscillation. *J. Clim.* **13**, 2550-2569 (2000)
- 853 Joyce, T. M., Zhang, R. On the path of the Gulf Stream and the Atlantic meridional overturning  
854 circulation. *J. Clim.*, **23**, 3146-3154, doi:10.1175/2010JCLI3310.1 (2010)  
855
- 856 Kay, S. M. *Modern spectral estimation: theory and application*. Prentice-Hall, Englewood  
857 Cliffs, NJ USA (1988)
- 858 Kelly, K. A., Small, R. J., Samelson, R. M., Qiu B., Joyce, T. M., Kwon, Y-O., & Cronin, M. F.  
859 Western boundary currents and frontal air-sea interaction: Gulf Stream and Kuroshio  
860 Extension. *J. Clim.*, **23**, 5644-5667, doi:10.1175/2010JCLI3346.1 (2010)
- 861 Lee, T. & Cornillon, P. Temporal variation of meandering intensity and domain-wide lateral  
862 oscillations of the Gulf Stream. *J. Geophys. Res.* **100**, 13603–13613 (1995)
- 863 Li, Y., Ji, R., Fratantoni, P. S., Chen, C., Hare, J. A., Davis, C. S. & Beardsley, R. C. Wind-  
864 induced inter-annual variability of sea level slope, alongshelf flow, and surface salinity on  
865 the Northwest Atlantic shelf, *J. Geophys. Res.* **119**, 2462–2479 (2014)
- 866 Marshall, J., Johnson, H., & Goodman, J. A study of the interaction of the North Atlantic  
867 oscillation and ocean circulation. *J. Clim.*, **14**, 1399-1421 (2001)  
868

- 868  
869 McCarthy, G., Frajka-Williams, E., Johns, W. E., Baringer, M. O., Meinen, C. S., Bryden, H. L.,  
870 Rayner, D., Ducez, A., Roberts, C., & Cunningham, S. A. Observed inter-annual  
871 variability of the Atlantic meridional overturning circulation at 26.5°N. *Geophys. Res.*  
872 *Lett.*, **39**, L19609, doi: 10.1029/2012GL052933 (2012)
- 873 Mountain, D. G. Variability in the properties of Shelf Water in the Middle Atlantic Bight, 1977-  
874 1999. *J. Geophys. Res.* **108**, doi:10.1029/2001JC001044 (2003)
- 875 Peña-Molino, B. and Joyce, T. M. Variability in the Slope Water and its relation to the Gulf  
876 Stream path. *Geophys. Res. Lett.* **35**, doi:10.1029/2007GL032183 (2008)
- 877 Perez-Hernandez, M. D., & Joyce, T. M. Two modes of Gulf Stream variability revealed in the  
878 last two decades of satellite altimeter data. *J. Phys. Oceanogr.* **44**, 149-163 (2014)
- 879 Pershing, A. J., Alexander, M. A., Hernandez, C. M., Kerr, L. A., Le Bris, A., Mills, K. E., Nye,  
880 J. A., Record, N. R., Scannell, H. A., Scott, J. D., Sherwood, G. D., Thomas, A. C. Slow  
881 adaptation in the face of rapid warming leads to collapse of the Gulf of Maine cod fishery.  
882 *Science* **350**, 809-812 (2015)
- 883 Rossby, T. On gyre interactions. *Deep-Sea Res. II* **46**, 139-164 (1999)
- 884 Rossby, T. & Benway, R. L. Slow variations in mean path of the Gulf Stream east of Cape  
885 Hatteras. *Geophys. Res. Lett.* **27**, 117-120 (2000)
- 886 Rossby, T., Flagg, C. N., Donohue, K., Sanchez-Franks, A. & Lillibridge, J. On the long-term  
887 stability of Gulf Stream transport based on 20 years of direct measurements. *Geophys. Res.*  
888 *Lett.* **41**, 114-120 (2014)
- 889 Sallenger, A. H., Doran, K. S. & Howd, P. A. Hotspot of accelerated sea level rise on the  
890 Atlantic coast of North America. *Nature Clim. Ch.* **2**, 884-888 (2012)
- 891 Sanchez-Franks, A., & Zhang R. Impact of the Atlantic Meridional Overturning Circulation on  
892 the decadal variability of the Gulf Stream path and regional chlorophyll and nutrient  
893 concentrations, *Geophys. Res. Lett.*, **42**, 9889–9887 (2015), doi:10.1002/2015GL066262.
- 894 Sanchez-Franks, A., Hameed, S., & Wilson, R. E. The Icelandic low as a predictor of the Gulf  
895 Stream north wall position. *J. Phys. Oceanogr.* **46**, 817-826 (2016)
- 896 Sato, O. T. & Rossby, T. Seasonal and low frequency variations in dynamic height and transport  
897 of the Gulf Stream. *Deep-Sea Res.* **42**, 149-164 (1995)
- 898 Shearman, R. K. & Lentz, S. J. Long-term sea surface temperature variability along the U.S. east  
899 coast. *J. Phys. Oceanogr.* **40**, 1004-1017 (2010)
- 900

- 900 Smeed, D. A., McCarthy, G. D., Cunningham, S. A., Frajka-Williams, E., Rayner, D., Johns,  
901 W. E., Meinen, C. S., Baringer, M. O., Moat, B. I., Ducheze, A., & Bryden, H. L.  
902 Observed decline of the Atlantic meridional overturning circulation 2004-2012. *Ocean*  
903 *Sci.* **10**, 29-38 (2014)  
904
- 905 Sundby, S. & Drinkwater, K. On the mechanisms behind salinity anomaly signals of the northern  
906 North Atlantic. *Prog. In Oceanogr.* **73**: 190-202 (2007)
- 907 Taylor, A. H. & Stephens, J. A. The North Atlantic Oscillation and the latitude of the Gulf  
908 Stream. *Tellus* **50A**: 134-142 (1998)
- 909 Toole, J. M., Curry, R. G., Joyce, T. M., McCartney, M. & Peña-Molino, B. Transport of the  
910 North Atlantic deep western boundary current about 39°N, 70°W: 2004-2008. *Deep-Sea*  
911 *Res. II* **58**, 1768-1780 (2011)
- 912 Watts, D. R. Gulf Stream variability. *Eddies in Marine Science*, A. R. Robinson, Ed., Springer-  
913 Verlag 114-167 (1983)
- 914 Wunsch, C. The interpretation of short climate records, with comments on the North Atlantic and  
915 Southern Oscillation. *Bull. Amer. Meteor. Soc.* **80**, 245-255 (1999)
- 916 Yashayaev, I., Seidov, D. & Demirov, E. A new collective view of oceanography of the Arctic  
917 and North Atlantic basins. *Prog. In Oceanogr.* **132**: 1-21 (2015)